minerals

MDPI

Article

Geochemical Characterization of Laminated Crystalline Crust Travertines Formed by Ca^{2+}-Deficient Hot Springs at Sobcha (China)

Zhipeng Lu [1,2], Huaguo Wen [1,2,3,4,*], Lianchao Luo [5], Liang Li [6] and Ying Nie [7]

1 State Key Laboratory of Oil and Gas Reservoir Geology and Exploitation, Chengdu University of Technology, Chengdu 610059, China
2 Institute of Sedimentary Geology, Chengdu University of Technology, Chengdu 610059, China
3 CNPC Key Laboratory of Carbonate Reservoir, Chengdu University of Technology, Chengdu 610059, China
4 Key Laboratory of Deep-Time Geographical Environment Reconstruction and Application, Ministry of Natural Resources, Chengdu 610059, China
5 Department of Earth Sciences, University of Florence, 50121 Firenze, Italy
6 College of Earth Sciences, Chengdu University of Technology, Chengdu 610059, China
7 School of Geoscience and Technology, Southwest Petroleum University, Chengdu 610500, China
* Correspondence: wenhuaguo08@cdut.edu.cn

Abstract: Travertines formed of crystalline crust have been widely reported, but there has not been focus on their geochemical characteristics. We therefore carefully conducted a series of geochemical investigations and U-Th dating on a travertine mound mainly composed of crystalline crust from Sobcha (southwest China) to determine their geochemical features and geological implications. The Sobcha travertines dominantly consist of granular crystals and fan crystals and show $\delta^{13}C$ from 3.4‰ to 4.9‰ V-PDB, $\delta^{18}O$ from −26.7‰ to −23.7‰ V-PDB, and $^{87}Sr/^{86}Sr$ from 0.712458 to 0.712951. When normalized to PASS, the Sobcha travertines exhibit MREE enrichment relative to HREE and LREE, HREE enrichment relative to LREE, and positive Eu anomalies. The $\delta^{13}C$ signatures and mother CO_2 evaluation of the Sobcha travertines show that the Sobcha travertines were thermogene travertines largely receiving mother CO_2 from (upper) mantle (i.e., magmatic CO_2) or a mixture of soil-derived CO_2 and CO_2 related to carbonate decarbonation. The $^{87}Sr/^{86}Sr$ of the Sobcha travertines is out of the $^{87}Sr/^{86}Sr$ ranges of local deposits exposed at Sobcha and surrounding areas but is well matched with the mean $^{87}Sr/^{86}Sr$ of Nadi Kangri volcanic rocks which cropped out to the northeast of the studied travertines (over 20 km away). This might indicate the important role of the Nadi Kangri volcanic rocks in suppling Sr to the studied travertines, but more studies are required. The LREE depletion compared to MREE and HREE in the Sobcha travertines was interpreted to be caused by the difference in geochemical mobility between LREEs and HREEs during water–rock interaction at depth, while the MREE enrichment compared to HREE was considered to be most likely inherited from reservoir/aquifer rocks. The positive Eu anomalies of the Sobcha travertines may result from very high reservoir temperatures and/or preferential dissolution of Eu-rich minerals/rocks (especially plagioclase). The Sobcha travertine mounds displays no or very slight vertical variations in $\delta^{13}C$, $^{87}Sr/^{86}Sr$, and REE patterns, indicating the compositional stability of mother CO_2 and paleo-fluids. However, a significant vertical increase in $\delta^{18}O$ was observed and was explained as the result of gradual water temperature decrease related to climate cooling, self-closure of the vents, or mound vertical growth. The findings in this study might help us better understand the deposition of crystalline crust in Ca^{2+}-deficient hot spring systems.

Keywords: travertine mound; crystalline crust; C-O-Sr isotopes; rare-earth elements; Tibet

check for updates

Citation: Lu, Z.; Wen, H.; Luo, L.; Li, L.; Nie, Y. Geochemical Characterization of Laminated Crystalline Crust Travertines Formed by Ca^{2+}-Deficient Hot Springs at Sobcha (China). *Minerals* **2023**, *13*, 220. https://doi.org/10.3390/min13020220

Academic Editors: Francesca Giustini, Mauro Brilli and Giovanni Ruggieri

Received: 18 November 2022
Revised: 29 January 2023
Accepted: 30 January 2023
Published: 2 February 2023

1. Introduction

Travertines (i.e., thermogene/hypogean travertines) are typical terrestrial carbonate rocks/deposits associated with warm-hot springs on the earth's surface [1]. Travertine

systems are often characterized by diverse morphologies, rapid changes of lithofacies and environments, rapid precipitation rates, and the deficiency of macrophytes and faunas [1–4]. More attention has recently been paid to travertines largely owing to their great potentials in enhancing our understanding of tectonic activity [5–15], paleo-climate [16–19], paleo-environment [16,17,20,21], thermal fluid circulation in geothermal systems [8,22], $CaCO_3$ polymorphism and crystallization [23–25], microbe-mediated carbonate precipitation [26–40], simulation of engineered geological storage and leakage of CO_2 [41,42], and pre-salt carbonate hydrocarbon reservoirs [43–45].

The lithofacies composition of travertines is quite complex [46,47], but one attractive lithofacies in many travertine systems is abiotic crystalline crust, which is formed of abundant well-packed bright calcite and/or aragonite crystals and often has a low porosity. Similar lithofacies in carbonate deposits from other environments (e.g., marine, lake) is commonly treated as diagenetic products. In contrast, abiotic crystalline crust in travertine systems is commonly considered to be primary deposits mainly formed by rapid passive CO_2 degassing [47–53]. However, calcite/aragonite crystals constituting abiotic crystalline crust shows various morphologies and sizes, such as dendritic crystals over 1 cm high, and raft-like crystals more than 5 cm long [49–52,54]. Therefore, abiotic crystalline crust is often further subdivided according to the morphology and size of the main fabrics. Gandin and Capezzuoli [47], for example, split abiotic crystalline crust in tufa and travertine systems up into five subtypes: feather-like/dendritic crystals, fan/ray crystals, banded palisade crystals, and foam rock and calcite rafts, which can be formed under numerous deposition conditions.

Many works on the sedimentological, petrological, and mineralogical characteristics of abiotic crystalline crust have been carried out over the past few decades [47–52,55–57]. Geochemical characteristics of travertines have also been investigated in some studies [58–61]. However, most of them only focused on the stable carbon and oxygen isotope compositions of travertines [52,61–67]. The $^{87}Sr/^{86}Sr$ and rare-earth elements signatures of travertines were poorly examined and interpreted in past studies. This study thus carefully characterized the geochemical compositions ($\delta^{13}C$, $\delta^{18}O$, $^{87}Sr/^{86}Sr$, and rare-earth elements) of laminated crystalline crust travertines at Sobcha, Tibet, southwestern China. Based on the geochemical results, this study attempted to determine the genesis, (paleo-)fluid source(s), and fluid evolution of the Sobcha travertine system. Some geochronological data were also obtained in this study. Considering that the Sobcha travertine system was likely deposited by hot springs deficient in Ca^{2+} (Ca^{2+} concentrations of active hot springs at Sobcha are 0.17 mM) [68], the findings obtained in this study might aid in the geochemical interpretation of crystalline crust travertines, especially those formed in Ca^{2+}-deficient hot spring systems.

2. Geological Setting

Sobcha is located in central Tibet, southwestern China (32°31′36.7″ N, 89°56′39″ E; altitude: ca. 4735 m) (Figure 1) and lies to the north of Qixiang Co Lake (ca. 2 km). The sedimentary sequences cropping out at Sobcha and surrounding areas mainly include (1) Upper Triassic–Lower Jurassic Sobcha Formation (also known as Xiaochaka Formation and Suobucha Formation) marine deposits mainly consisting of limestone, (2) Lower Jurassic Quse Formation and Middle Jurassic Sewa Formation marine deposits mainly composed of clastic deposits (e.g., shale, sandstone, and claystone), and (3) Neogene and Quaternary terrestrial clastic deposits [69–71]. A series of E–W faults developed at Sobcha and surrounding areas. The studied travertines were formed on the Upper Triassic–Lower Jurassic Sobcha Formation marine deposits and are situated very close to two faults (Figure 1).

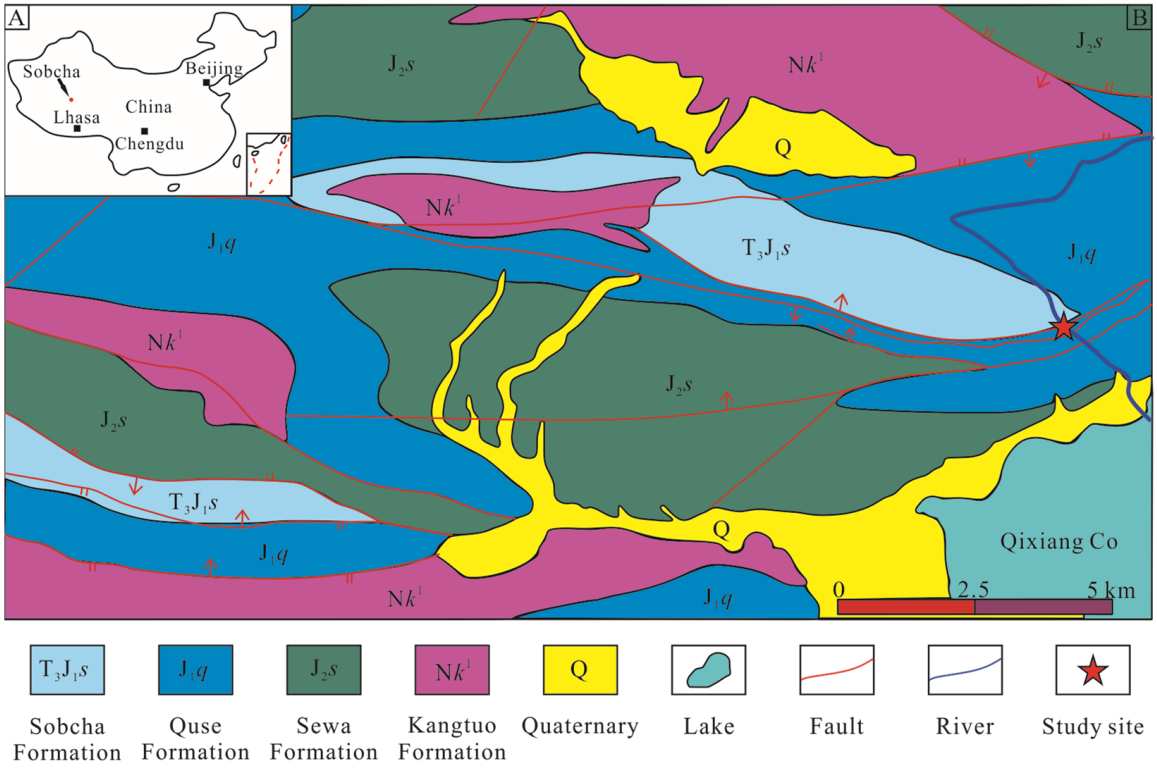

Figure 1. (**A**) The location of Sobcha in the Tibetan Plateau, southwestern China. (**B**) Simplified geological map of the study area (modified from Fu et al. [70]).

The studied Sobcha travertines are fossil travertine deposits, but modern hot springs and associated deposits, though very limited, are still present near the studied travertines. Liao [68] called this place Quse or Sobcha Hot Fountain. Specifically, this place is a hot spring area composed of 12 vents [68]. The location information of these hot spring vents given by Liao [68] is very close to that of the Sobcha travertines (89°56′25″ E, 32°31′35″ N; altitude: 4770 m). A pioneering study by Liao [68] showed that most of the hot springs at Sobcha have vent temperatures from 45 °C to 50 °C and only two hot springs at Sobcha show vent temperatures near 60 °C. The water composition of one hot spring was also reported by Liao [68]: pH = 8.62, Ca^{2+} concentration = 0.17 mM, Mg^{2+} concentration = 0.69 mM, K^+ concentration = 0.87 mM, Na^+ concentration = 22.17 mM, HCO_3^- concentration = 14.95 mM, SO_4^{2-} concentration = 1.58 mM, Cl^- concentration = 3.55 mM, and CO_3^{2-} concentration = 1.68 mM. Na^+ is absolutely dominant in the cation composition. Thus, the studied fossil travertines were anticipated to be formed by Ca^{2+}-deficient hot springs, similar to those in Tengchong (China) [72], Lake Bogoria (Kenya) [73], and Waikite (New Zealand) [74].

3. Methods

Fifty-eight fossil travertines samples were collected in the field. Specific sampling sites for geochemical analysis are shown in Figure 2D. To evaluate their mineralogical composition, thirty powder samples were made using an agate motor and a pestle and were then analyzed with a DX-2700 X-ray diffractometer (XRD) (Cu-Kα radiation; 2θ from 5° to 60°). Fifty-eight thin sections were prepared and were observed with a Nikon LV100POL polarizing microscope to check the petrographic and mineralogical features of the Sobcha travertines. Both the XRD and thin section analyses were conducted at Chengdu University of Technology, China.

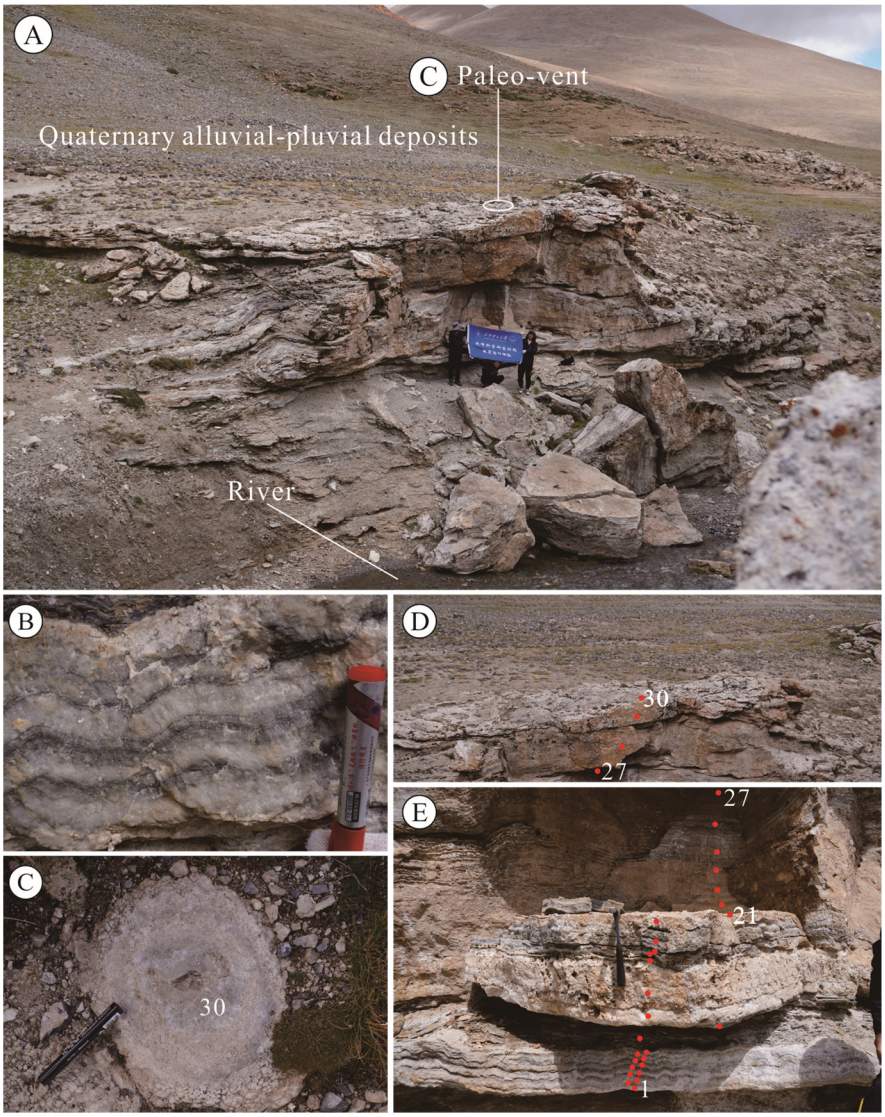

Figure 2. (**A**) General view of the studied travertine mound at Sobcha. (**B**) Nearly horizontal laminated abiotic crystalline crust travertines; (**C**) Paleo-vent situated at the top of the studied travertine mound (its location can be found in panel (**A**)). (**D**,**E**) Schematic diagram of sampling sites of the Sobcha travertines for geochemical analysis. The red dots represent the sample site for geochemical analysis, the number represents the sample number, and the same number represents the same sample.

$\delta^{13}C$, $\delta^{18}O$, $^{87}Sr/^{86}Sr$, and concentrations of some trace elements (including rare-earth elements, manganese, strontium, zirconium, copper) of the Sobcha travertines were examined to determine the genesis of the travertines and the characteristics of paleo-fluids. Travertine samples used for geochemical analyses were ground into powder using an agate motor and a pestle and the powder samples were then sifted using a 200 mesh sieve. $\delta^{13}C$ and $\delta^{18}O$ signatures were determined for thirty samples using a Thermo Fisher Scientific DELTA V Advantage isotope ratio mass spectrometer and their values were reported relative to the Vienna Pee Dee Belemnite standard (V-PDB). The analytical precision is commonly better than 0.2‰ for $\delta^{13}C$ and 0.3‰ for $\delta^{18}O$. $^{87}Sr/^{86}Sr$ values were determined for thirty travertine samples using a Thermo Fisher Scientific Triton Plus mass spectrometer. The final $^{87}Sr/^{86}Sr$ results were corrected by assuming a non-radiogenic $^{86}Sr/^{88}Sr$ isotopic ratio of 0.1194. Rare-earth elements (i.e., REE), Mn, Sr, Zr, and Cu concentrations were determined for twenty travertine samples using a Jena Plasma Quant MS ICP-MS. U-Th dating of three travertine samples collected from the bottom (Sample 1),

middle (Sample 21), and top (Sample 30) of the sampling profile at Sobcha, respectively, was also conducted using a Neptune Plus MC-ICP-MS. The $\delta^{13}C$-$\delta^{18}O$ analyses, $^{87}Sr/^{86}Sr$ analyses, trace element analyses, and U-Th dating were completed at Yangtze University (China), Chengdu University of Technology (China), Beijing Createch Testing Technology Co., Ltd. (Beijing, China), and the Institute of Geology and Geophysics (Chinese Academy of Sciences), respectively.

In this study, rare-earth elements were divided into three groups: light REE (i.e., LREE: La, Ce, Pr, and Nd), middle REE (i.e., MREE: Sm, Eu, Gd, Tb, Dy, and Ho), and heavy REE (i.e., HREE: Er, Tm, Yb, and Lu) [75]. To better interpret REE characteristics of the Sobcha travertines, REE of Post-Archean Australian Shale (PAAS) [76] was utilized to normalize the REE values of the studied travertines. Additionally, anomalies of Eu were presented as $(Eu/Eu^*)_N$, and were calculated using the following equations: $(Eu/Eu^*)_N = Eu_N/(Sm_N^2 \times Tb_N)^{1/3}$ [77]. The relative enrichments of LREE, MREE, and HREE were presented as $(Pr/Yb)_N$ (LREE compared to HREE), $(Pr/Tb)_N$ (LREE compared to MREE), and $(Tb/Yb)_N$ (MREE compared to HREE) [75].

4. Results

4.1. Description of the Sobcha Travertines

The studied travertine system is a domical mound system developed on a slightly inclined slope (Figure 2), morphologically similar to the travertine mounds found in Chusang (southwestern China) [78]. It is characterized by an asymmetric outline with a nearly flat surface at the upslope side and a relatively steep surface at the downslope side. An orifice which had been nearly fully sealed was found on the top surface of the mound (Figure 2C). Determining the exact scale of the mound system was handicapped by the fact that some of the travertine mound was covered by clastic deposits and/or soils and that fluvial incision eroded parts of the travertine mound (Figure 2A). However, the residual travertines were observed to be at least over twenty meters wide. The fluvial incision was largely caused by a north-flowing river (i.e., Sobcha River). Due to the fluvial incision, a four-meter-high travertine profile was exposed, providing a good place for our field observation and sampling.

4.2. Petrology and Mineralogy

The outcropping travertines at Sobcha show great laminated structures, which are characterized by the alternation of wavy dark laminae and wavy light laminae (Figure 2B). Both dark laminae and wavy light laminae have highly variable thicknesses, but in general, light laminae are thicker and more dominant. Furthermore, the Sobcha travertines are consolidated and show visible large calcite crystals ranging from 1 to 10 mm in hand specimens. Large cavities (up to 2 cm in diameter) are also visible in the outcrop, but their development is very limited in fresh samples. Therefore, these cavities are largely secondary (probably generated by the dissolution of meteoric water or temporary flood water).

According to the lithofacies classification of Gandin and Capezzuoli [47], most of the Sobcha travertines are identified as (abiotic) crystalline crust. In this study, the Sobcha travertines were termed 'laminated crystalline crust' to clearly indicate their textural and petrological characteristics. Apart from the laminated crystalline crust, a small amount of clotted peloidal boundstone was also observed in the studied travertine system. XRD and thin-section analyses shows the predominance of calcite in both the laminated crystalline crust and the clotted peloidal boundstone.

The clotted peloidal boundstone is formed of dark micrite peloids and sparite (Figure 3A), while components constituting the laminated crystalline crust include fan crystals and granular crystals (Figure 3B,C). The fan crystals range from 0.2 to 2 mm long and usually develop as thin layers ca. 30 mm thick (Figure 3B,C). The granular crystals are the most widely developed crystals in the Sobcha travertines and have highly variable sizes between 0.1 and 0.5 mm in diameter (Figure 3B). The granular crystals have a more irregular morphology and are subhedral to anhedral in shape (Figure 3B).

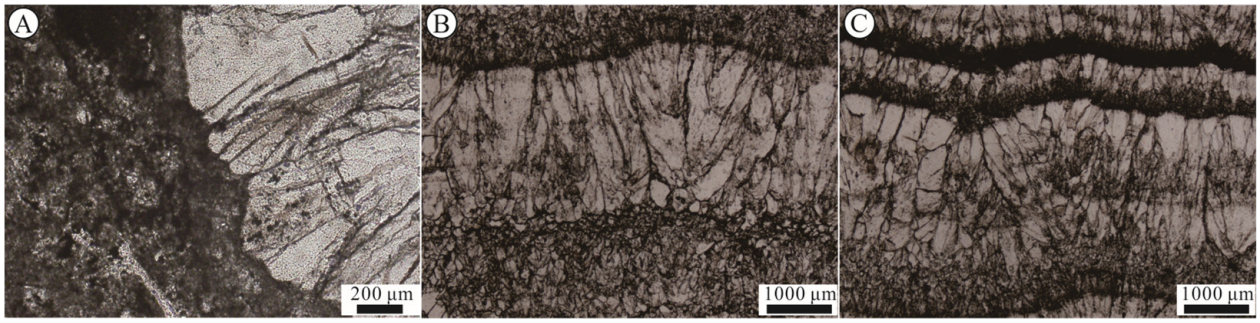

Figure 3. Thin-section microphotographs of the Sobcha travertines (**A**–**C**); plane-polarized light. (**A**) Clotted peloidal boundstone and fan crystals. (**B**) Fan crystals and granular crystals. (**C**) Fan crystals.

4.3. $\delta^{13}C$, $\delta^{18}O$, and $^{87}Sr/^{86}Sr$

The $\delta^{13}C$, $\delta^{18}O$, and $^{87}Sr/^{86}Sr$ signatures of the Sobcha travertines are listed in Table S1. The Sobcha travertines show $\delta^{13}C$ from 3.4‰ to 4.9‰ V-PDB (average = 4.0‰ V-PDB). $\delta^{18}O$ of the Sobcha travertines has a range larger than $\delta^{13}C$ (from −26.7‰ to −23.7‰ V-PDB, average = −25.6‰ V-PDB). A positive $\delta^{13}C$-$\delta^{18}O$ correlation was found in the Sobcha travertines, but the correlation is not very strong (R^2 = 0.50, n = 30) (Figure 4). Additionally, it is notable that there is a gradual positive $\delta^{18}O$ shift from the bottom to the top of the studied profile, although a few anomalous values are also present (Figure 5A). Such increase was also found in $\delta^{13}C$ of the travertines, but the $\delta^{13}C$ excursion is very slight (Figure 5B). Unlike visible $\delta^{13}C$ and $\delta^{18}O$ variations, $^{87}Sr/^{86}Sr$ of the Sobcha travertines are nearly unchanged and show a very narrow range from 0.712458 to 0.712951 (average = 0.712737, n = 30) (Figure 5C).

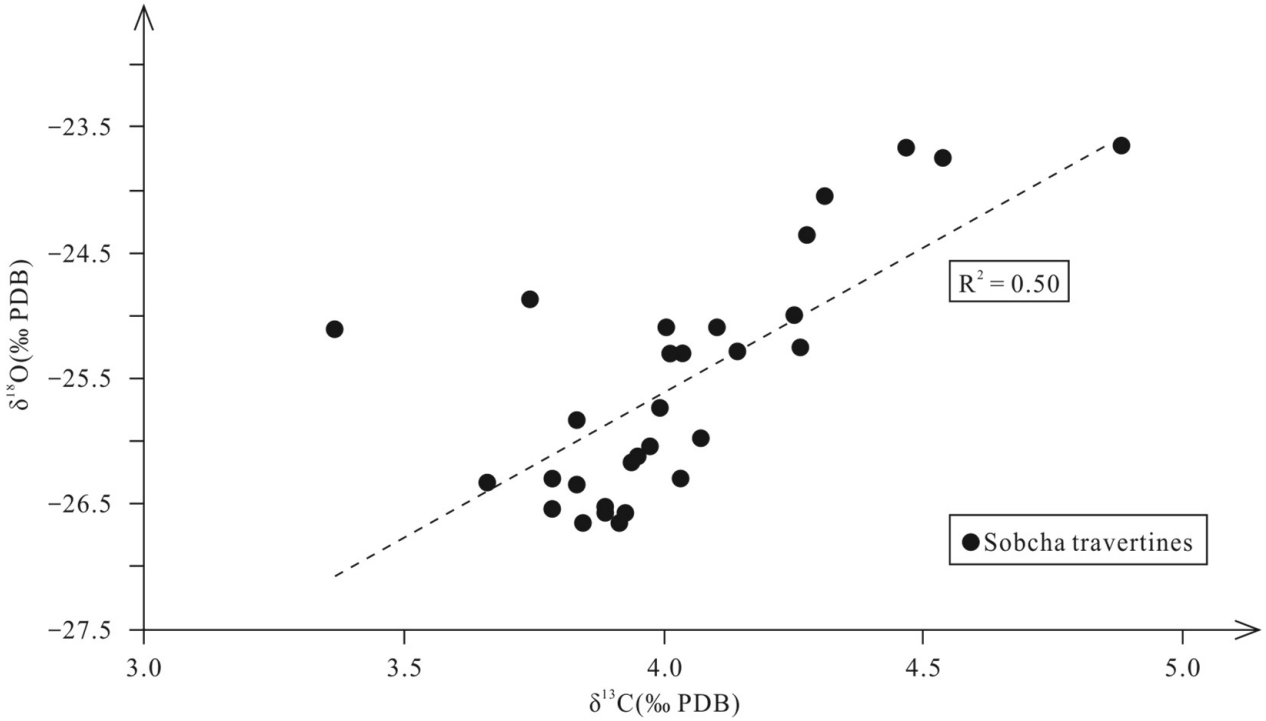

Figure 4. Bivariant graph of $\delta^{18}O$ and $\delta^{13}C$ of travertines from Sobcha.

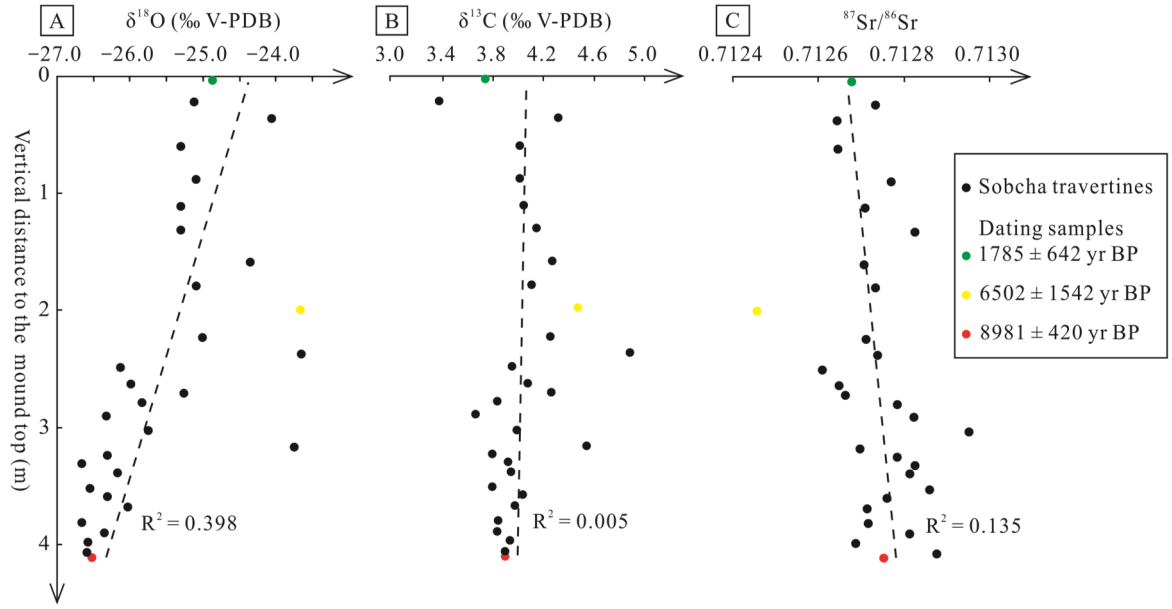

Figure 5. (**A**–**C**) Vertical variations of $\delta^{18}O$, $\delta^{13}C$, and $^{87}Sr/^{86}Sr$ of the Sobcha travertines in the studied profile.

4.4. U-Th Dating

The U-Th dating results of three travertine samples (i.e., Samples 1, 21, and 30) are listed in Table S2. Samples 1, 21, and 30 were collected from the bottom, middle, and top of the sampling profile at Sobcha, respectively. Sample 1 has a measured depositional age of 8981 ± 420 yr BP, while Sample 21 exhibits a depositional age of 6502 ± 1542 yr BP. Sample 30 is the youngest of the three samples and its corrected age is 1785 ± 642 yr BP. The dating results show that travertine deposition of the studied travertine mound system began, at least, in the early Holocene and ceased in the late Holocene.

4.5. Rare-Earth Elements, Mn, Sr, Zr, and Cu

Rare-earth elements, Mn, Sr, Zr, and Cu concentrations and some main calculated geochemical parameters of the Sobcha travertines are listed in Tables S3 and S4. ΣREE of the Sobcha travertines is highly variable (ranging from 0.61 to 23.05 μg g^{-1}, average = 8.04 μg g^{-1}), but most of the samples show ΣREE below 13.00 μg g^{-1}. The Sobcha travertines show significant MREE and HREE enrichment relative to LREE, as shown by their very low $(Pr/Tb)_N$ (from 0.10 to 0.55, mostly between 0.10 and 0.25, average = 0.16) and $(Pr/Yb)_N$ (from 0.12 to 0.60, commonly between 0.12 and 0.24, average = 0.19). $(Tb/Yb)_N$ ratios of the Sobcha travertines vary from 1.09 to 1.21 (average = 1.14), indicating the Sobcha travertines are weakly MREE-enriched compared to HREE.

Elemental anomaly calculations show that the Sobcha travertines have $(Eu/Eu^*)_N$ ratios range from 1.05 to 1.68 (average = 1.36) and most of the $(Eu/Eu^*)_N$ data are between 1.28 and 1.43. This reflects unneglectable positive Eu anomalies in the Sobcha travertines.

The Sobcha travertines have very low Zr and Mn concentrations and Mn/Sr ratios. Their Zr concentrations are from 0.38 to 3.24 μg g^{-1} (average = 1.73 μg g^{-1}), but most of the values are lower than 2 μg g^{-1}. Mn concentrations of the Sobcha travertines are between 279 and 1280 μg g^{-1} and have an average value of 825.75 μg g^{-1}. The calculated Mn/Sr ratios are within a small range from 0.53 to 2.48 (average = 1.63). Cu concentrations of the Sobcha travertines are between 0.19 and 1.17 μg g^{-1} and have an average value of 0.52 μg g^{-1}.

5. Interpretation and Discussion

5.1. Interpretation of $\delta^{13}C$: Source of Mother CO_2

$\delta^{13}C$ analyses of travertines are good tools in the determination of mother CO_2 sources [52,62,79]. $\delta^{13}C$ of mother CO_2 (i.e., $\delta^{13}C_{mother\text{-}CO2}$) of spring-related carbonates have been used to divide them into thermogene travertine and meteogene travertine [79–83]. For example, according to Pentecost and Viles [83], $\delta^{13}C$ of thermogene travertines ranges from −4‰ to 8‰ V-PDB, whereas $\delta^{13}C$ of meteogene travertines ranges from −11‰ to 0 V-PDB. $\delta^{13}C$ values of the Sobcha travertines are between 3.4‰ and 4.9‰ V-PDB, which is obviously in the $\delta^{13}C$ range of thermogene travertines. In addition, Figure 6 also shows that the Sobcha travertines belongs to hypogean CATT (calcitic or aragonitic travertine and tufa) [60]. However, spring-related carbonates with $\delta^{13}C$ in the travertine range may show highly different CO_2 sources. Thus, $\delta^{13}C_{mother\text{-}CO2}$ of the Sobcha travertines were calculated and compared with $\delta^{13}C$ of potential CO_2 sources to determine their genesis and mother CO_2 source(s).

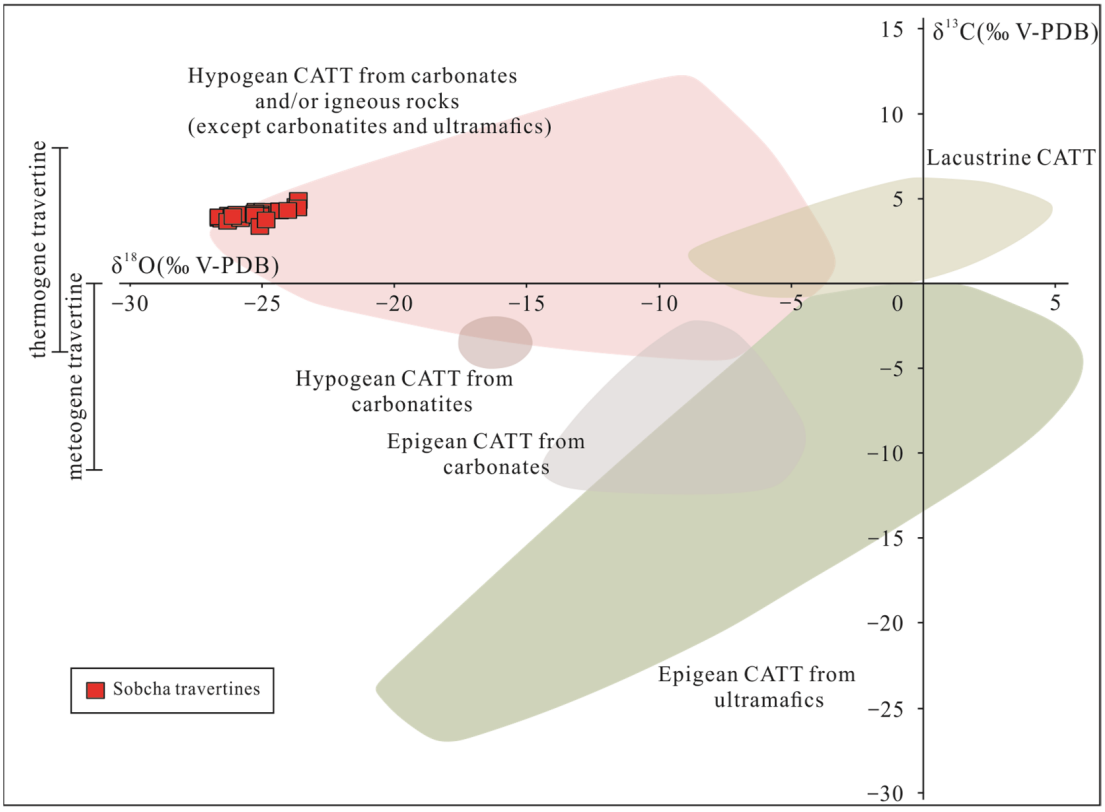

Figure 6. $\delta^{13}C$ and $\delta^{18}O$ composition for the Sobcha travertines. $\delta^{13}C$ ranges for thermogene and meteogene travertines were from Pentecost and Viles [64]. $\delta^{13}C$ and $\delta^{18}O$ ranges of different CATT (i.e., calcitic or aragonitic travertine and tufa) were from Teboul et al. [65].

The empirical equation developed by Panichi and Tongiorgi [84] was adapted to calculate $\delta^{13}C_{mother\text{-}CO2}$ of the Sobcha travertines. The calculated $\delta^{13}C_{mother\text{-}CO2}$ varies from −6.5‰ and −4.6‰ V-PDB (Table S1). A simple comparison in Figure 7 shows that the calculated $\delta^{13}C_{mother\text{-}CO2}$ overlaps the $\delta^{13}C$ range of mantle-derived CO_2, and is significantly different from $\delta^{13}C$ of soil-related CO_2 and $\delta^{13}C$ of marine carbonate rocks in the study area and surrounding areas [69,85–88]. This might be indicative of the close relationship between the Sobcha travertines and mantle-derived CO_2. Such magmatic CO_2-containing volatiles has been found in hot springs from Naqu (close to the study area) and was interpreted as the product of magma bodies in the shallow crust [89,90]. Unfortunately,

detailed analyses of hot spring gases from the study area have not been performed. Thus, such a mantle-derived CO_2 origin is possible but is not the only interpretation.

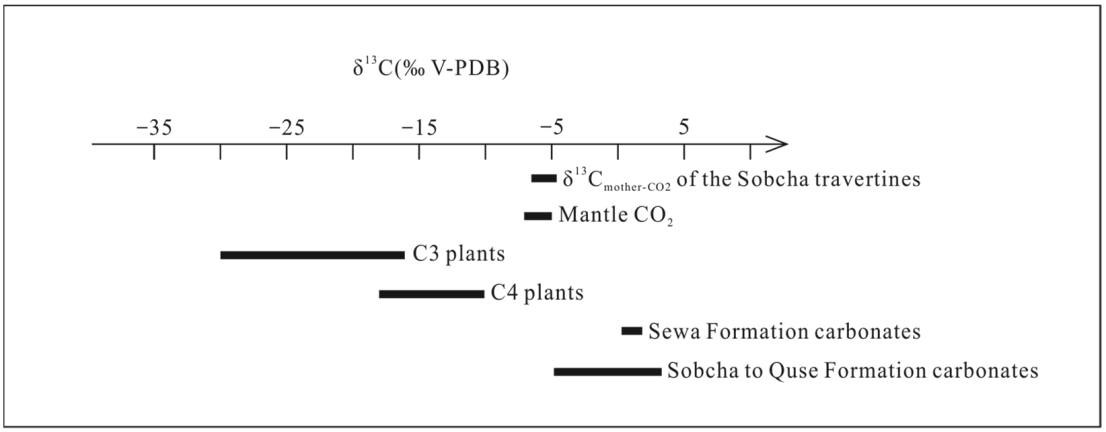

Figure 7. Calculated $\delta^{13}C_{mother\text{-}CO2}$ of the Sobcha travertines in comparison with $\delta^{13}C$ of potential carbon sources. $\delta^{13}C$ ranges of mantle-derived CO_2 and CO_2 related to C3 plants and C4 plants were from Vogel [69] and Prokoph et al. [68]. $\delta^{13}C$ ranges of carbonate rocks of the Sewa Formation and Sobcha to Quse Formation were from Yi [70] and Yi [49]; Fu et al. [67]; Yi [70].

An alternative explanation of the similarity between the calculated $\delta^{13}C_{mother\text{-}CO2}$ range and $\delta^{13}C$ of mantle-derived CO_2 is underground CO_2 mixing. Apart from magmatic CO_2, there are at least two main CO_2 sources for travertine systems: soil CO_2 (C3 or C4 plants) and carbonate-related CO_2 (either by the dissolution or decarbonation of carbonate rocks) [82]. In our study area, the distribution of C4 plants is very limited, probably due to its high altitude [91]. Therefore, the plants in the study area are mainly C3 plants. For the carbonate-related CO_2, given the low Ca^{2+} concentration (0.17 mM) and high HCO_3^- concentrations (14.95 mM) of the modern spring in the study area [68], the dissolution of carbonate rocks is considered to only supply minor CO_2 to the spring waters and travertines at Sobcha. However, this cannot exclude the CO_2 contribution of carbonate decarbonization because this process can provide CO_2 to the spring water (in other words, elevating HCO_3^- concentration) without increasing the concentrations of Ca^{2+} and Mg^{2+}. If there was an underground mixing between soil CO_2 and carbonate-related CO_2, their mixture may yield similar $\delta^{13}C$ to mantle-derived CO_2. Thus, mixing, if present, might happen between soil CO_2 (C3 plants) and CO_2 related to carbonate decarbonation.

5.2. Interpretation of $^{87}Sr/^{86}Sr$: Sr Source Rocks

The $^{87}Sr/^{86}Sr$ analysis of travertines can be used to determine their Sr sources [72]. With respect to the studied travertines, all the rocks exposing in the study area are their potential Sr source rocks. A simple comparison between $^{87}Sr/^{86}Sr$ of the studied travertines and $^{87}Sr/^{86}Sr$ of potential Sr source rocks [92–94] was made and is given in Figure 8. The comparison shows that the $^{87}Sr/^{86}Sr$ range of the Sobcha travertines is significantly higher than $^{87}Sr/^{86}Sr$ ranges of carbonate rocks and clastic rocks exposed in/near the study area (mainly the Quse Formation) and Cambrian to Cenozoic marine carbonates (Figure 8). This suggests that the studied travertines must acquire more radiogenic Sr from other Sr source rocks, instead of from the local rocks cropping out in the study area. Interestingly, the studied travertines display $^{87}Sr/^{86}Sr$ very close to the average $^{87}Sr/^{86}Sr$ value of Nadi Kangri volcanic rocks. However, the nearest exposed Nadi Kangri volcanic rocks are located in the Bilong Co area and are ca. 20 km away from the study area [95]. Thus, simply treating the Nadi Kangri volcanic rocks as the main Sr source rocks of the studied travertines is not very appropriate. Conclusively, further studies are required to uncover the main Sr source rocks of the Sobcha travertines.

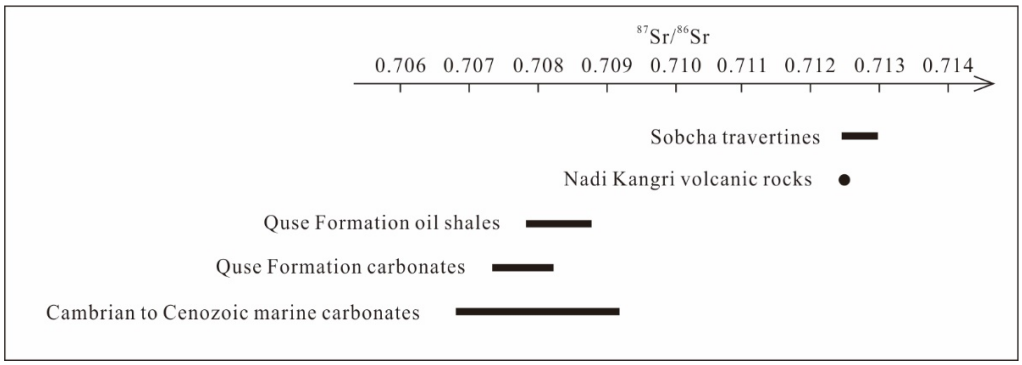

Figure 8. $^{87}Sr/^{86}Sr$ in the studied travertines in comparison with $^{87}Sr/^{86}Sr$ ranges of potential Sr source rocks: oil shales and micritic limestones of the Quse Formation (data from Fu et al. [76]), average values of Nadi Kangri volcanic rocks (data from Fu et al. [75]), and Cambrian to Cenozoic marine carbonates (data from McArthur et al. [77]).

5.3. Interpretation of REE Patterns and Eu Anomalies

REE of carbonate rocks might not be pristine, because they can be easily contaminated by other materials, such as clastic detritus [96–103] and Fe-Mn (oxyhydr) oxides [104] during or after deposition. Thus, prior to the analysis of REE of carbonates, a contaminant evaluation is often required. The Sobcha travertines shows Zr concentrations lower than 4 μg g^{-1} (Table S3). This indicates that there is no significant contamination from clastic detritus [98]. In addition, the Sobcha travertines display no Cu–ΣREE correlations and have very low Mn concentrations (279 to 1660 μg g^{-1}) (Table S3, Figure 9), reflecting that the contamination of Fe-Mn (oxyhydr)oxides is not important [105]. The REE modification of post-depositional processes can be also neglected because the Mn/Sr ratios of the Sobcha travertines are all less than 3 (Table S4) [106–108]. These show that our REE data are not significantly contaminated and can provide original geological information.

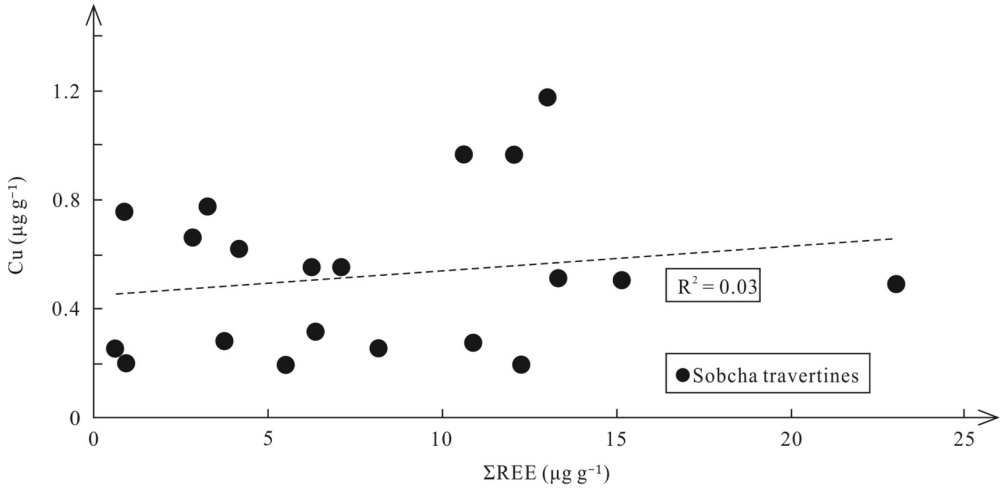

Figure 9. Bivariant graph of Cu and ΣREE of travertines from Sobcha.

There are two striking REE characteristics of the Sobcha travertines: (1) MREE-enrichment relative to both HREE and LREE and HREE-enrichment relative to LREE, and (2) positive Eu anomalies (1.28 and 1.43; Figure 10 and Table S4). There are two main factors which might influence REE patterns of the studied travertine: solution complexation and REE of aquifer rocks. Paleo-fluids depositing the Sobcha travertines might be compositionally similar to active hot springs at Sobcha (i.e., bicarbonate- and carbonate-rich) [68]. Such fluids could form strong HREE-complexes (i.e., preferential HREE incorporation into fluids) and the resulting fluids and associated deposits would be HREE-enriched compared to REE of their aquifer rocks [109]. However, it is strange that although the Sobcha

travertines are HREE-enriched compared to LREE, their HREE are depleted compared to MREE. This indicates that their MREE-enrichment was largely inherited from aquifer rocks, instead of caused by solution complexation. However, this does not mean that the influence of solution complexation on the REE pattern of the Sobcha travertines is very weak. It is here believed that solution complexation might indeed cause the HREE-enrichment in the Sobcha travertines, but such HREE-enrichment did not fully mask the aquifer rock REE information recorded in the travertines (i.e., MREE-enrichment). In Figure 11 the REE patterns of the Sobcha travertines are compared with those of rocks cropping out in the study area, such as shale, calci-mudstone, and marl of the Quse Formation and Nadi Kangri volcanic rocks (including basalt, rhyolite, dacite, and tuff) [70,110–115]. It is clear that none of the surface rocks display MREE-enrichment, excluding the possibility that these rocks are aquifer rocks. Such inference is consistent with the results of the $^{87}Sr/^{86}Sr$ analyses in Section 5.2 because aquifer rocks were often considered as predominant Sr source rocks [116–118].

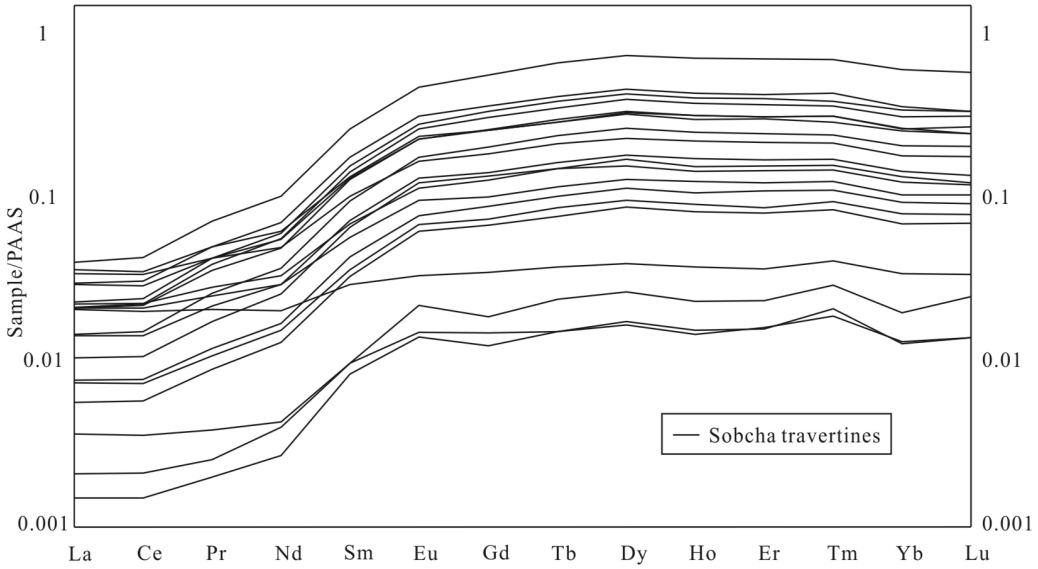

Figure 10. PAAS-normalized REE patterns for the travertine samples of Sobcha.

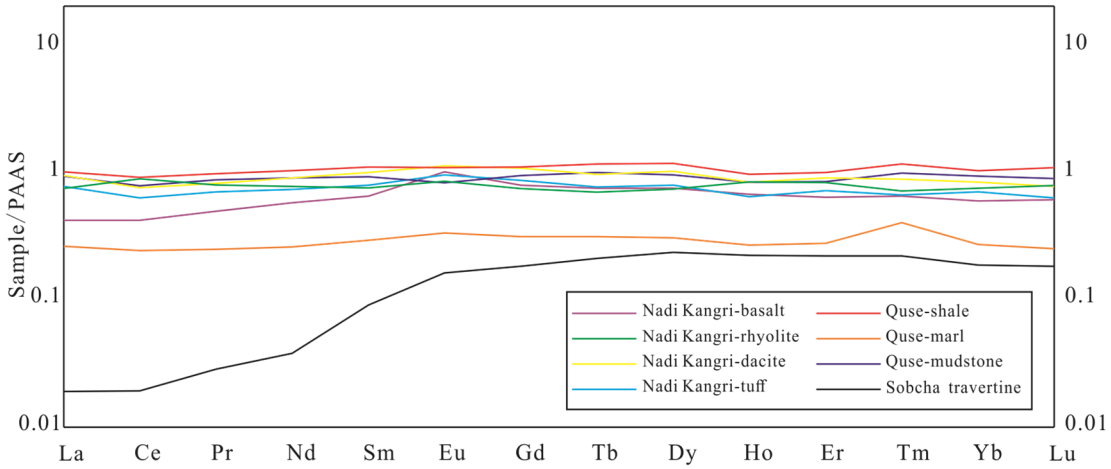

Figure 11. Comparison of PAAS-normalization patterns between Sobcha travertines and potential source rocks: basalt, rhyolite, and dacite of the Nadi Kangri volcanic rocks (data from Fu et al. [93]); tuff of the Nadi Kangri volcanic rocks (data from Wang et al. [96]; Fu et al. [97]; Wang et al. [98]); shale of the Quse Formation (data from Fu et al. [50]); mudstone of the Quse Formation (data from Nie et al. [95]); and marl of the Quse Formation (data from Fu et al. [94]).

Positive Eu anomalies in marine carbonate rocks are often indicative of a hydrothermal origin of their parent fluids [75,119]. At high temperatures (often >250 °C), Eu might be fractionated from other REE because of the reduction of Eu into Eu^{2+} [120], which would finally cause Eu enrichment in high-temperature fluids. As a result, carbonate rocks deposited from these fluids, or their cooled products might show positive Eu anomalies. At Sobcha, the temperature of its reservoir(s) has not been investigated. However, geothermal systems with reservoir temperatures over 250 °C have been found in Central Tibet (e.g., Yangbajing geothermal field) [121]. Therefore, it is possible that positive Eu anomalies of the Sobcha travertines might be related to undiscovered high-temperature reservoirs beneath Sobcha. An alternative explanation of the positive Eu anomalies in the Sobcha travertines might be the preferential dissolution of Eu-rich minerals/rocks (especially plagioclase). Indeed, such a process is not uncommon in groundwater systems [122]. Therefore, positive Eu anomalies of the studied travertines might be caused by high-temperature geothermal reservoir(s), preferential dissolution of Eu-rich minerals/rocks, or both, and more studies are still necessary in this region.

5.4. Evolution of Paleo-Fluids

Travertine deposition may be affected by various factors, such as tectonic activity, climate, hydrodynamics, and hydrochemistry [10,12,17,123] and is thus not always steady. For example, some of these complex controlling factors (either internal or external), such as climate change, may lead to the changes in the flow path and/or discharge. However, changes in (paleo-)fluids (e.g., the source and physicochemical properties of the mother water) might be reflected by the geochemical features of travertine deposits, such as $\delta^{13}C$, $^{87}Sr/^{86}Sr$, and REE. The $\delta^{13}C$ of the Sobcha travertines shows a great stability (Table S1, Figure 5B). The small range of $\delta^{13}C$ indicates that the CO_2 source of the Sobcha travertines did not change. The $^{87}Sr/^{86}Sr$ and REE signatures of the Sobcha travertines also display little changes in the sampling profile (Table S1 and Figure 5C), indicating the source and physicochemical stability of the mother water of the Sobcha travertines

The $\delta^{18}O$ of the Sobcha travertines has a larger variation than $\delta^{13}C$ and shows a striking gradual increase from bottom to top of the sampling profile (Table S1 and Figure 5A). The $\delta^{18}O$ signature of travertines is important to the recovery of paleo-temperature of the mother water in travertine deposition systems [52,62,79]. We were unable to recover the exact temperature changes of the mother water depositing the Sobcha travertines. However, according to common traditional oxygen isotope thermometers, there is an inverse relationship between $\delta^{18}O$ of carbonate deposits and water temperature [124]. Thus, the positive $\delta^{18}O$ excursion in the studied travertine profile of Sobcha, at least, indicates that paleo-fluid temperature forming the Sobcha travertines decreased gradually. However, the factors that cause such a $\delta^{18}O$ increase or temperature decrease remain unknown.

Climate (mainly atmospheric temperature and rainfall) may influence the temperature of mother water of travertines [63,64,125]. The Sobcha travertine deposition began, at least, in the early Holocene and ceased in the late Holocene. From the early Holocene to the middle Holocene and to the late Holocene, the southern Qinghai–Tibet Plateau was generally in a climate background from drought to humid and to drought, as recorded in the $\delta^{18}O$ composition of cave deposits [126–128]. In the Holocene, the temperature of the Qinghai–Tibet Plateau also experienced a gradual increase from the early to the middle period and a gradual decrease from the middle to the late period [126]. In general, the trend of $\delta^{18}O$ during the deposition period of the Sobcha travertines are similar to that of $\delta^{18}O$ recorded in cave deposits of the southern Qinghai–Tibet Plateau at the same time. This seems to indicate that the $\delta^{18}O$ of the Sobcha travertines, or rather the temperature of the mother water, is affected by climate.

In addition to climate, a gradual decrease in the discharge of the mother water may also lead to a faster decrease in the temperature of the mother water (assuming the air temperature is stable). This would in turn lead to a gradual increase in the $\delta^{18}O$ of the deposits. The gradual decrease in the discharge of the mother water of the Sobcha travertines may

also be due to the gradual drought of the climate during the deposition period. However, the self-closure of the vents and mound vertical growth might also lead to a gradual decrease in water discharge of mound springs. For the Sobcha travertines, we found that the paleo-vent was completely closed due to the growth of deposit (Figure 2C). Therefore, it is possible that water discharge of paleo-fluids depositing the Sobcha travertines gradually decreased due to the gradual closure of the vent(s) and/or mound vertical growth.

6. Conclusions

Through the geochemical and geochronological study on the Sobcha fossil travertine mound, we mainly draw the following conclusions:

(1) The Sobcha travertines are dominantly composed of laminated crystalline crust mainly composed of granular crystals and fan crystals. In addition, a small amount of clotted peloidal boundstone was also observed. Calcite has an absolute predominance in the Sobcha travertines.

(2) $\delta^{13}C$ and $\delta^{18}O$ analyses show that the Sobcha travertines belong to thermogene travertines, and its parent CO_2 may be derived from mantle-derived CO_2 or the mixture of soil-derived CO_2 and CO_2 related to carbonate decarbonation.

(3) The Sobcha travertines display $^{87}Sr/^{86}Sr$ very close to the average $^{87}Sr/^{86}Sr$ value of Nadi Kangri volcanic rocks. However, further studies are required to uncover the main Sr source rocks of the Sobcha travertines.

(4) For the PAAS-normalized REE patterns of the Sobcha travertines, the LREE depletion relative to HREE of the Sobcha travertines may be due to the differences in geochemical mobility between LREEs and HREEs during water–rock interaction at depth, while the MREE enrichment of the Sobcha travertines may be inherited from aquifer rocks. Positive Eu anomalies were also observed in the Sobcha travertines and may result from the hydrothermal property of the mother water and/or preferential dissolution of Eu-rich minerals/rocks.

(5) Travertine deposition in the studied travertine mound began, at least, in the early Holocene and ceased in the late Holocene. During the whole deposition period, the source of CO_2 and the source of the mother water of Sobcha travertines remained stable. However, $\delta^{18}O$ of the studied travertines gradually decreased, probably because of climate drying, self-closure of the vents, or mound vertical growth.

Supplementary Materials: The following supporting information can be downloaded at https://www.mdpi.com/article/10.3390/min13020220/s1. Table S1: $\delta^{13}C$, $\delta^{18}O$, and $^{87}Sr/^{86}Sr$ values of the Sobcha travertines and their calculated $\delta^{13}C_{mother\text{-}CO2}$ (i.e., $\delta^{13}C$ of mother CO_2). $\delta^{13}C_{mother\text{-}CO2}$ was evaluated using the equation from Panichi and Tongiorgi [84]. Table S2: U-Th dating results of the Sobcha travertines. Table S3: Concentrations (μg $g^{-}1$) of trace elements in the travertine samples from Sobcha. Table S4: Mn/Sr, enrichment indexes, and elemental anomalies of the studied travertines from Sobcha.

Author Contributions: Conceptualization, Z.L., H.W. and L.L. (Lianchao Luo); methodology, Z.L., H.W. and L.L. (Lianchao Luo); software, Z.L. and L.L. (Lianchao Luo); validation, Z.L., H.W. and L.L. (Lianchao Luo); formal analysis, Z.L. and L.L. (Lianchao Luo); investigation, Z.L., L.L. (Liang Li), and Y.N.; resources, H.W.; data curation, H.W.; writing—original draft preparation, Z.L.; writing—review and editing, Z.L., H.W., L.L. (Lianchao Luo), L.L. (Liang Li), and Y.N.; visualization, Z.L. and L.L. (Lianchao Luo); supervision, H.W.; project administration, H.W.; funding acquisition, H.W. All authors have read and agreed to the published version of the manuscript.

Funding: This research was funded by the National Natural Science Foundation of China (grant number 41972116 and 41572097 to H. Wen).

Data Availability Statement: Not applicable.

Acknowledgments: We are grateful to Mingshi Fen (Chengdu University of Technology) for his help in SEM analyses, Di Yang (Chengdu University of Technology) for her help in Sr isotope analyses, and Miao Deng (Chengdu University of Technology) for his help in XRD analyses, Xiugen Fu (Southwest Petroleum University) for his help in field survey, and Xuefeng Wang (Uranium chronology laboratory, Institute of Geology and Geophysics, Chinese Academy of Sciences) for his help in U-Th dating analyses.

Conflicts of Interest: The authors declare no conflict of interest.

References

1. Capezzuoli, E.; Gandin, A.; Pedley, M. Decoding tufa and travertine (fresh water carbonates) in the sedimentary record: The state of the art. *Sedimentology* **2014**, *61*, 1–21. [CrossRef]
2. Ford, T.D.; Pedley, H.M. A review of tufa and travertine deposits of the world. *Earth-Sci. Rev.* **1996**, *41*, 117–175. [CrossRef]
3. Pedley, M. Tufas and travertines of the Mediterranean region: A testing ground for freshwater carbonate concepts and developments. *Sedimentology* **2009**, *56*, 221–246. [CrossRef]
4. Wen, H.; Luo, L.; Luo, X.; You, Y.; Du, L. Advances and Prospects of Terrestrial Thermal Spring Travertine Research. *Acta Sedimentol. Sin.* **2019**, *37*, 1162–1180, (In Chinese with English Abstract).
5. Altunel, E.; Hancock, P.L. Morphology and structural setting of Quaternary travertines at Pamukkale, Turkey. *Geol. J.* **1993**, *28*, 335–346. [CrossRef]
6. Altunel, E.; Hancock, P.L. Structural Attributes of Travertine-Filled Extensional Fissures in the Pamukkale Plateau, Western Turkey. *Int. Geol. Rev.* **1996**, *38*, 768–777. [CrossRef]
7. Altunel, E.; Karabacak, V. Determination of horizontal extension from fissure-ridge travertines: A case study from the Denizli Basin, southwestern Turkey. *Geodin. Acta* **2005**, *18*, 333–342. [CrossRef]
8. Brogi, A.; Alcicek, M.C.; Yalciner, C.C.; Capezzuoli, E.; Liotta, D.; Meccheri, M.; Rimondi, V.; Ruggieri, G.; Gandin, A.; Boschi, C.; et al. Hydrothermal fluids circulation and travertine deposition in an active tectonic setting: Insights from the Kamara geothermal area (western Anatolia, Turkey). *Tectonophysics* **2016**, *680*, 211–232. [CrossRef]
9. Brogi, A.; Capezzuoli, E. Travertine deposition and faulting: The fault-related travertine fissure-ridge at Terme S. Giovanni, Rapolano Terme (Italy). *Int. J. Earth Sci.* **2009**, *98*, 931–947. [CrossRef]
10. Brogi, A.; Capezzuoli, E. Earthquake impact on fissure-ridge type travertine deposition. *Geol. Mag.* **2014**, *151*, 1135–1143. [CrossRef]
11. Brogi, A.; Liotta, D.; Capezzuoli, E.; Matera, P.F.; Kele, S.; Soligo, M.; Tuccimei, P.; Ruggieri, G.; Yu, T.L.; Shen, C.C.; et al. Travertine deposits constraining transfer zone neotectonics in geothermal areas: An example from the inner Northern Apennines (Bagno Vignoni-Val d'Orcia area, Italy). *Geothermics* **2020**, *85*, 22. [CrossRef]
12. Gradzinski, M.; Wroblewski, W.; Dulinski, M.; Hercman, H. Earthquake-affected development of a travertine ridge. *Sedimentology* **2014**, *61*, 238–263. [CrossRef]
13. Hancock, P.L.; Chalmers, R.M.L.; Altunel, E.; Cakir, Z. Travitonics: Using travertines in active fault studies. *J. Struct. Geol.* **1999**, *21*, 903–916. [CrossRef]
14. Selim, H.H.; Yanik, G. Development of the Cambazli (Turgutlu/MANISA) fissure-ridge-type travertine and relationship with active tectonics, Gediz Graben, Turkey. *Quat. Int.* **2009**, *199*, 157–163. [CrossRef]
15. Shiraishi, F.; Morikawa, A.; Kuroshima, K.; Amekawa, S.; Yu, T.-L.; Shen, C.-C.; Kakizaki, Y.; Kano, A.; Asada, J.; Bahniuk, A.M. Genesis and diagenesis of travertine, Futamata hot spring, Japan. *Sediment. Geol.* **2020**, *405*, 105706. [CrossRef]
16. Prado-Perez, A.J.; Huertas, A.D.; Crespo, M.T.; Sanchez, A.M.; Del Villar, L.P. Late Pleistocene and Holocene mid-latitude palaeoclimatic and palaeoenvironmental reconstruction: An approach based on the isotopic record from a travertine formation in the Guadix-Baza basin, Spain. *Geol. Mag.* **2013**, *150*, 602–625. [CrossRef]
17. Rodriguez-Berriguete, A.; Alonso-Zarza, A.M. Controlling factors and implications for travertine and tufa deposition in a volcanic setting. *Sediment. Geol.* **2019**, *381*, 13–28. [CrossRef]
18. Toker, E.; Kayseri-Ozer, M.S.; Ozkul, M.; Kele, S. Depositional system and palaeoclimatic interpretations of Middle to Late Pleistocene travertines: Kocaba, Denizli, south-west Turkey. *Sedimentology* **2015**, *62*, 1360–1383. [CrossRef]
19. Uysal, I.T.; Unal-Imer, E.; Shulmeister, J.; Zhao, J.X.; Karabacak, V.; Feng, Y.X.; Bolhar, R. Linking CO_2 degassing in active fault zones to long-term changes in water balance and surface water circulation, an example from SW Turkey. *Quat. Sci. Rev.* **2019**, *214*, 164–177. [CrossRef]
20. Camuera, J.; Alonso-Zarza, A.M.; Rodriguez-Berriguete, A.; Rodriguez-Gonzalez, A. Origin and palaeo-environmental significance of the Berrazales carbonate spring deposit, North of Gran Canaria Island, Spain. *Sediment. Geol.* **2014**, *308*, 32–43. [CrossRef]
21. Kele, S.; Korpás, L.; Demény, A.; Kovács-Pálffy, P.; Bajnóczi, B.; Medzihradszky, Z. Paleoenvironmental evaluation of the Tata Travertine Complex (Hungary), based on stable isotopic and petrographic studies. *Acta Geol. Hung.* **2006**, *49*, 1–31. [CrossRef]

22. Capezzuoli, E.; Ruggieri, G.; Rimondi, V.; Brogi, A.; Liotta, D.; Alcicek, M.C.; Alcicek, H.; Bulbul, A.; Gandin, A.; Meccheri, M.; et al. Calcite veining and feeding conduits in a hydrothermal system: Insights from a natural section across the Pleistocene Golemezli travertine depositional system (western Anatolia, Turkey). *Sediment. Geol.* **2018**, *364*, 180–203. [CrossRef]
23. Jones, B. Review of aragonite and calcite crystal morphogenesis in thermal spring systems. *Sediment. Geol.* **2017**, *354*, 9–23. [CrossRef]
24. Jones, B. Review of calcium carbonate polymorph precipitation in spring systems. *Sediment. Geol.* **2017**, *353*, 64–75. [CrossRef]
25. Luo, L.C.; Capezzuoli, E.; Rogerson, M.; Vaselli, O.; Wen, H.G.; Lu, Z.P. Precipitation of carbonate minerals in travertine-depositing hot springs: Driving forces, microenvironments, and mechanisms. *Sediment. Geol.* **2022**, *438*, 27. [CrossRef]
26. Fouke, B.W. Hot-spring Systems Geobiology: Abiotic and biotic influences on travertine formation at Mammoth Hot Springs, Yellowstone National Park, USA. *Sedimentology* **2011**, *58*, 170–219. [CrossRef]
27. Guo, L.I.; Riding, R. Origin and diagenesis of Quaternary travertine shrub fabrics, Rapolano Terme, central Italy. *Sedimentology* **1994**, *41*, 499–520. [CrossRef]
28. Jones, B.; Peng, X.T. Signatures of biologically influenced CaCo3 and Mg-Fe silicate precipitation in hot springs: Case study from the Ruidian geothermal area, western Yunnan Province, China. *Sedimentology* **2014**, *61*, 56–89. [CrossRef]
29. Rogerson, M.; Pedley, H.M.; Kelham, A.; Wadhawan, J.D. Linking mineralisation process and sedimentary product in terrestrial carbonates using a solution thermodynamic approach. *Earth Surf. Dyn.* **2014**, *2*, 197–216. [CrossRef]
30. Shiraishi, F.; Eno, Y.; Nakamura, Y.; Hanzawa, Y.; Asada, J.; Bahniuk, A.M. Relative influence of biotic and abiotic processes on travertine fabrics, Satono-yu hot spring, Japan. *Sedimentology* **2019**, *66*, 459–479. [CrossRef]
31. Sugihara, C.; Yanagawa, K.; Okumura, T.; Takashima, C.; Harijoko, A.; Kano, A. Transition of microbiological and sedimentological features associated with the geochemical gradient in a travertine mound in northern Sumatra, Indonesia. *Sediment. Geol.* **2016**, *343*, 85–98. [CrossRef]
32. Takashima, C.; Kano, A. Microbial processes forming daily lamination in a stromatolitic travertine. *Sediment. Geol.* **2008**, *208*, 114–119. [CrossRef]
33. Della Porta, G.; Hoppert, M.; Hallmann, C.; Schneider, D.; Reitner, J. The influence of microbial mats on travertine precipitation in active hydrothermal systems (Central Italy). *Depos. Rec.* **2022**, *8*, 165–209. [CrossRef]
34. Norris, T.B.; Castenholz, R.W. Endolithic photosynthetic communities within ancient and recent travertine deposits in Yellowstone National Park. *FEMS Microbiol. Ecol.* **2006**, *57*, 470–483. [CrossRef] [PubMed]
35. Okumura, T.; Takashima, C.; Shiraishi, F.; Nishida, S.; Yukimura, K.; Naganuma, T.; Koike, H.; Arp, G.; Kano, A. Microbial Processes Forming Daily Lamination in an Aragonite Travertine, Nagano-yu Hot Spring, Southwest Japan. *Geomicrobiol. J.* **2011**, *28*, 135–148. [CrossRef]
36. Okumura, T.; Takashima, C.; Shiraishi, F.; Nishida, S.; Kano, A. Processes Forming Daily Lamination in a Microbe-Rich Travertine Under Low Flow Condition at the Nagano-yu Hot Spring, Southwestern Japan. *Geomicrobiol. J.* **2013**, *30*, 910–927. [CrossRef]
37. Okumura, T.; Takashima, C.; Kano, A. Textures and processes of laminated travertines formed by unicellular cyanobacteria in Myoken hot spring, southwestern Japan. *Island Arc.* **2013**, *22*, 410–426. [CrossRef]
38. Okumura, T.; Takashima, C.; Shiraishi, F.; Akmaluddin; Kano, A. Textural transition in an aragonite travertine formed under various flow conditions at Pancuran Pitu, Central Java, Indonesia. *Sediment. Geol.* **2012**, *265–266*, 195–209. [CrossRef]
39. Takashima, C.; Okumura, T.; Nishida, S.; Shimamoto, T.; Koike, H.; Kano, A. Microbial Control on Lamina Formation in a Travertine of Crystal Geyser, Utah. In *Advances in Stromatolite Geobiology*; Reitner, J., Quéric, N.-V., Arp, G., Eds.; Springer: Berlin/Heidelberg, Germany, 2011; pp. 123–133.
40. Valeriani, F.; Crognale, S.; Protano, C.; Gianfranceschi, G.; Orsini, M.; Vitali, M.; Spica, V.R. Metagenomic analysis of bacterial community in a travertine depositing hot spring. *New Microbiol.* **2018**, *41*, 126–135.
41. Burnside, N.M.; Shipton, Z.K.; Dockrill, B.; Ellam, R.M. Man-made versus natural CO_2 leakage: A 400 k.y. history of an analogue for engineered geological storage of CO_2. *Geology* **2013**, *41*, 471–474. [CrossRef]
42. Moore, J.; Adams, M.; Allis, R.; Lutz, S.; Rauzi, S. Mineralogical and geochemical consequences of the long-term presence of CO_2 in natural reservoirs: An example from the Springerville-St. Johns Field, Arizona, and New Mexico, USA. *Chem. Geol.* **2005**, *217*, 365–385. [CrossRef]
43. Chafetz, H.; Barth, J.; Cook, M.; Guo, X.; Zhou, J. Origins of carbonate spherulites: Implications for Brazilian Aptian pre-salt reservoir. *Sediment. Geol.* **2018**, *365*, 21–33. [CrossRef]
44. Mancini, A.; Capezzuoli, E.; Erthal, M.; Swennen, R. Hierarchical approach to define travertine depositional systems: 3D conceptual morphological model and possible applications. *Mar. Pet. Geol.* **2019**, *103*, 549–563. [CrossRef]
45. Ronchi, P.; Cruciani, F. Continental carbonates as a hydrocarbon reservoir, an analog case study from the travertine of Saturnia, Italy. *AAPG Bull.* **2015**, *99*, 711–734. [CrossRef]
46. Della Porta, G. Carbonate build-ups in lacustrine, hydrothermal and fluvial settings: Comparing depositional geometry, fabric types and geochemical signature. *Geol. Soc. Lond. Spec. Publ.* **2015**, *418*, 17–68. [CrossRef]
47. Gandin, A.; Capezzuoli, E. Travertine: Distinctive depositional fabrics of carbonates from thermal spring systems. *Sedimentology* **2014**, *61*, 264–290. [CrossRef]

48. Alcicek, M.C.; Alcicek, H.; Altunel, E.; Arenas, C.; Bons, P.; Brogi, A.; Capezzuoli, E.; de Riese, T.; Della Porta, G.; Gandin, A.; et al. Comment on "First records of syn-diagenetic non-tectonic folding in Quaternary thermogene travertines caused by hydrothermal incremental veining" by Billi et al. Tectonophysics 700–701 (2017) 60–79. *Tectonophysics* **2017**, *721*, 491–500. [CrossRef]
49. Jones, B.; Peng, X.T. Intrinsic versus extrinsic controls on the development of calcite dendrite bushes, Shuzhishi Spring, Rehai geothermal area, Tengchong, Yunnan Province, China. *Sediment. Geol.* **2012**, *249*, 45–62. [CrossRef]
50. Jones, B.; Renaut, R.W. Cyclic development of large, complex, calcite dendrite crystals in the Clinton travertine, Interior British Columbia, Canada. *Sediment. Geol.* **2008**, *203*, 17–35. [CrossRef]
51. Jones, B.; Renaut, R.W.; Owen, R.B.; Torfason, H. Growth patterns and implications of complex dendrites in calcite travertines from Lysuholl, Sn ae fellsnes, Iceland. *Sedimentology* **2005**, *52*, 1277–1301. [CrossRef]
52. Luo, L.C.; Wen, H.G.; Li, Y.; You, Y.X.; Luo, X.T. Mineralogical, crystal morphological, and isotopic characteristics of smooth slope travertine deposits at Reshuitang, Tengchong, China. *Sediment. Geol.* **2019**, *381*, 29–45. [CrossRef]
53. Kano, A.; Okumura, T.; Takashima, C.; Shiraishi, F. *Geomicrobiological Properties and Processes of Travertine: With a Focus on Japanese Sites*; Springer: Singapore, 2019.
54. Jones, B.; Peng, X.T. Hot spring deposits on a cliff face: A case study from Jifei, Yunnan Province, China. *Sediment. Geol.* **2014**, *302*, 1–28. [CrossRef]
55. Chafetz, H.S.; Folk, R.L. Travertines; depositional morphology and the bacterially constructed constituents. *J. Sediment. Res.* **1984**, *54*, 289–316. [CrossRef]
56. Chafetz, H.S.; Guidry, S.A. Deposition and diagenesis of Mammoth Hot Springs travertine, Yellowstone National Park, Wyoming, U.S.A. *Can. J. Earth Sci.* **2003**, *40*, 1515–1529. [CrossRef]
57. Jones, B.; Renaut, R.W. Noncrystallographic Calcite Dendrites from Hot-Spring Deposits at Lake Bogoria, Kenya. *J. Sediment. Res. Sect. A-Sediment. Petrol. Process.* **1995**, *65*, 154–169.
58. Olsson, J.; Stipp, S.L.S.; Gislason, S.R. Element scavenging by recently formed travertine deposits in the alkaline springs from the Oman Semail Ophiolite. *Mineral. Mag.* **2014**, *78*, 1479–1490. [CrossRef]
59. Qin, J.; Han, P.; Che, X.; Yuan, G.; Fang, B.; Wang, G. Resuming the Holocene paleoclimate using delta~(18)O and trace elements of travertine in Rongma area, Tibet. *Earth Sci. Front.* **2014**, *21*, 312–322.
60. Teboul, P.A.; Durlet, C.; Gaucher, E.C.; Virgone, A.; Girard, J.P.; Curie, J.; Lopez, B.; Camoin, G.F. Origins of elements building travertine and tufa: New perspectives provided by isotopic and geochemical tracers. *Sediment. Geol.* **2016**, *334*, 97–114. [CrossRef]
61. Porras-Toribio, I.; Pi-Puig, T.; Villanueva-Estrada, R.E.; Rubio-Ramos, M.A.; Sole, J. Mineralogy, Geochemistry, and Stable Isotopes (C, O, S) of Hot Spring Waters and Associated Travertines near Tamiahua Lagoon, Veracruz, Gulf of Mexico (Mexico). *Minerals* **2022**, *12*, 822. [CrossRef]
62. Jones, B.; Peng, X.T. Mineralogical, crystallographic, and isotopic constraints on the precipitation of aragonite and calcite at Shigiang and other hot springs in Yunnan Province, China. *Sediment. Geol.* **2016**, *345*, 103–125. [CrossRef]
63. Liu, Z.H.; Li, H.C.; You, C.F.; Wan, N.J.; Sun, H.L. Thickness and stable isotopic characteristics of modern seasonal climate-controlled sub-annual travertine laminas in a travertine-depositing stream at Baishuitai, SW China: Implications for paleoclimate reconstruction. *Environ. Geol.* **2006**, *51*, 257–265. [CrossRef]
64. Sun, H.; Liu, Z. Wet–dry seasonal and spatial variations in the $\delta^{13}C$ and $\delta^{18}O$ values of the modern endogenic travertine at Baishuitai, Yunnan, SW China and their paleoclimatic and paleoenvironmental implications. *Geochim. Cosmochim. Acta* **2010**, *74*, 1016–1029. [CrossRef]
65. Blasco, M.; Auque, L.F.; Gimeno, M.J.; Asta, M.P.; Mandado, J. Stable isotope characterisation of recent aragonite travertine deposits associated with the Fitero thermal waters (Spain). *Int. J. Earth Sci.* **2020**, *109*, 877–892. [CrossRef]
66. Kele, S.; Ozkul, M.; Forizs, I.; Gokgoz, A.; Baykara, M.O.; Alcicek, M.C.; Nemeth, T. Stable isotope geochemical study of Pamukkale travertines: New evidences of low-temperature non-equilibrium calcite-water fractionation. *Sediment. Geol.* **2011**, *238*, 191–212. [CrossRef]
67. Mohammadzadeh, H.; Daneshvar, M.R.M. A comparison of hydro-geochemistry and stable isotope composition of travertine-depositing springs, Garab in NE Iran and Pamukkale in SW Turkey. *Carbonates Evaporites* **2020**, *35*, 23. [CrossRef]
68. Liao, Z.J. *Thermal Springs and Geothermal Energy in the Qinghai-Tibetan Plateau and the Surroundings*; Springer: Singapore, 2018.
69. Yi, F. Carbon Isotopic Records and Its Paleoenvironmental Significance during the Triassic-jurassic Transition. in Qiangtang Area, Tibet. Ph.D. Thesis, Chengdu University of Technology, Chengdu, China, 2018. (In Chinese with English Abstract).
70. Fu, X.G.; Wang, J.; Chen, W.B.; Feng, X.L.; Wang, D.; Song, C.Y.; Zeng, S.Q. Elemental geochemistry of the early Jurassic black shales in the Qiangtang Basin, eastern Tethys: Constraints for palaeoenvironment conditions. *Geol. J.* **2016**, *51*, 443–454. [CrossRef]
71. Wang, Y.S.; Zheng, C.Z. Lithostratigraphy, Sequence Stratigraphy, and Biostratigraphy of the Su-Obucha and Quse Formations and the Triassic-Jurassic Boundary in The Sewa Area on The South Margin of the Qiangtang Basin, Northern Tibet. *J. Stratigr.* **2007**, *31*, 377–384, (In Chinese with English Abstract).
72. Luo, L.C.; Wen, H.G.; Capezzuoli, E. Travertine deposition and diagenesis in Ca-deficiency perched hot spring systems: A case from Shihuadong, Tengchong, China. *Sediment. Geol.* **2021**, *414*, 17. [CrossRef]
73. Jones, B.; Renaut, R.W.; Rosen, M.R. High-temperature (>90 degrees C) calcite precipitation at Waikite Hot Springs, North Island, New Zealand. *J. Geol. Soc.* **1996**, *153*, 481–496. [CrossRef]

74. Renaut, R.W.; Owen, R.B.; Jones, B.; Tiercelin, J.J.; Tarits, C.; Ego, J.K.; Konhauser, K.O. Impact of lake-level changes on the formation of thermogene travertine in continental rifts: Evidence from Lake Bogoria, Kenya Rift Valley. *Sedimentology* **2013**, *60*, 428–468. [CrossRef]
75. Zhao, Y.Y.; Wei, W.; Santosh, M.; Hu, J.; Wei, H.T.; Yang, J.; Liu, S.; Zhang, G.L.; Yang, D.D.; Li, S.Z. A review of retrieving pristine rare earth element signatures from carbonates. *Paleogeogr. Paleoclimatol. Paleoecol.* **2022**, *586*, 18. [CrossRef]
76. McLennan, S.M. *Rare Earth Elements in Sedimentary Rocks: Influence of Provenance and Sedimentary Processes*; De Gruyter: Berlin, Germany, 1989. [CrossRef]
77. Lawrence, M.G.; Greig, A.; Collerson, K.D.; Kamber, B.S. Rare earth element and yttrium variability in South East Queensland waterways. *Aquat. Geochem.* **2006**, *12*, 39–72. [CrossRef]
78. Wang, Z.J.; Meyer, M.C.; Hoffmann, D.L. Sedimentology, petrography and early diagenesis of a travertine-colluvium succession from Chusang (southern Tibet). *Sediment. Geol.* **2016**, *342*, 218–236. [CrossRef]
79. Jones, B.; Peng, X.T. Growth and development of spring towers at Shiqiang, Yunnan Province, China. *Sediment. Geol.* **2017**, *347*, 183–209. [CrossRef]
80. Kele, S.; Vaselli, O.; Szabó, C.; Minissale, A. Stable isotope geochemistry of Pleistocene travertine from Budakalász (Buda Mts, Hungary). *Acta Geol. Hung.* **2003**, *46*, 161–175. [CrossRef]
81. Pentecost, A. The quaternary travertine deposits of Europe and Asia Minor. *Quat. Sci. Rev.* **1995**, *14*, 1005–1028. [CrossRef]
82. Pentecost, A. *Travertine*; Springer: Berlin/Heidelberg, Germany, 2005.
83. Pentecost, A.; Viles, H. A Review and Reassessment of Travertine Classification. *Géographie Phys. et Quat.* **1994**, *48*, 305–314. [CrossRef]
84. Panichi, C.; Tongiorgi, E.; Panichi, C.; Tongiorgi, E. Carbon isotopic composition of CO_2 from springs, fumaroles, mofettes and travertines of central and southern Italy: A preliminary prospection method of geothermal areas. In Proceedings of the Second United Nations Symposium on the Development and Use of Geothermal, San Francisco, CA, USA, 20 May 1975; Volume 2, pp. 815–825.
85. Fu, X.G.; Wang, J.; Wen, H.G.; Song, C.Y.; Wang, Z.W.; Zeng, S.Q.; Feng, X.L.; Wei, H.Y. A Toarcian Ocean Anoxic Event record from an open-ocean setting in the eastern Tethys: Implications for global climatic change and regional environmental pertur-bation. *Sci. China Earth Sci.* **2021**, *64*, 1860–1872, (In Chinese with English Abstract). [CrossRef]
86. Prokoph, A.; Shields, G.A.; Veizer, J. Compilation and time-series analysis of a marine carbonate $\delta^{18}O$, $\delta^{13}C$, $^{87}Sr/^{86}Sr$ and $\delta^{34}S$ database through Earth history. *Earth-Sci. Rev.* **2008**, *87*, 113–133. [CrossRef]
87. Vogel, J.C. 4—Variability of Carbon Isotope Fractionation during Photosynthesis. In *Stable Isotopes and Plant Carbon-Water Relations*; Ehleringer, J.R., Hall, A.E., Farquhar, G.D., Eds.; Academic Press: San Diego, CA, USA, 1993; pp. 29–46.
88. Yi, H.S. The carbon isotope fluctuation and its origin interpretion during the Early to Middle Jurassic transition period in the Shuanghu area of Qiangtang Basin. *Sediment. Geol. Tethyan Geol.* **2021**, *41*, 505–511, (In Chinese with English Abstract).
89. Luo, M.; Huang, H.G.; Zhang, P.; Wu, Q.H.; Chen, D.F. Origins of gas discharging from the Qiangtang Basin in the northern Qinghai-Tibet Plateau, China: Evidence from gas compositions, helium, and carbon isotopes. *J. Geochem. Explor.* **2014**, *146*, 119–126. [CrossRef]
90. Yokoyama, T.; Nakai, S.i.; Wakita, H. Helium and carbon isotopic compositions of hot spring gases in the Tibetan Plateau. *J. Volcanol. Geotherm. Res.* **1999**, *88*, 99–107. [CrossRef]
91. Wang, R.Z.; Ma, L.N. Climate-driven C4 plant distributions in China: Divergence in C4 taxa. *Sci. Rep.* **2016**, *6*, 27977. [CrossRef] [PubMed]
92. Fu, X.G.; Wang, J.; Tan, F.W.; Feng, X.L.; Chen, W.B.; Song, C.Y.; Zeng, S.Q. Sr and Nd isotopic systematics of mid-cretaceous organic-rich rocks (oil shales) from the qiangtang basin: Implications for source regions and sedimentary paleoenvironment. *Oil Shale* **2015**, *32*, 109–123. [CrossRef]
93. Fu, X.G.; Wang, J.; Zeng, Y.H.; Tan, F.W.; Feng, X.L. Source regions and the sedimentary paleoenvironment of marine oil shale from the bilong co area, Northern Tibet, China: An SR-ND isotopic study. *Oil Shale* **2012**, *29*, 306–321. [CrossRef]
94. McArthur, J.M.; Howarth, R.J.; Shields, G.A.; Zhou, Y. Chapter 7—Strontium Isotope Stratigraphy. In *The Geologic Time Scale*; Gradstein, F.M., Ogg, J.G., Schmitz, M.D., Ogg, G.M., Eds.; Elsevier: Boston, MA, USA, 2012; pp. 127–144.
95. Hu, F.Z.; Fu, X.G.; Lin, L.; Song, C.Y.; Wang, Z.W.; Tian, K.Z. Marine Late Triassic-Jurassic carbon-isotope excursion and biological extinction records: New evidence from the Qiangtang Basin, eastern Tethys. *Glob. Planet. Change* **2020**, *185*, 103093. [CrossRef]
96. Bolhar, R.; Van Kranendonk, M.J. A non-marine depositional setting for the northern Fortescue Group, Pilbara Craton, inferred from trace element geochemistry of stromatolitic carbonates. *Precambrian Res.* **2007**, *155*, 229–250. [CrossRef]
97. Elderfield, H.; Upstill-Goddard, R.; Sholkovitz, E.R. The rare earth elements in rivers, estuaries, and coastal seas and their significance to the composition of ocean waters. *Geochim. et Cosmochim. Acta* **1990**, *54*, 971–991. [CrossRef]
98. Frimmel, H.E. Trace element distribution in Neoproterozoic carbonates as palaeoenvironmental indicator. *Chem. Geol.* **2009**, *258*, 338–353. [CrossRef]
99. Goldstein, S.J.; Jacobsen, S.B. Rare earth elements in river waters. *Earth Planet. Sci. Lett.* **1988**, *89*, 35–47. [CrossRef]
100. Nothdurft, L.D.; Webb, G.E.; Kamber, B.S. Rare earth element geochemistry of Late Devonian reefal carbonates, canning basin, Western Australia: Confirmation of a seawater REE proxy in ancient limestones. *Geochim. Et Cosmochim. Acta* **2004**, *68*, 263–283. [CrossRef]

101. Olivier, N.; Boyet, M. Rare earth and trace elements of microbialites in Upper Jurassic coral- and sponge-microbialite reefs. *Chem. Geol.* **2006**, *230*, 105–123. [CrossRef]
102. Van Kranendonk, M.J.; Webb, G.E.; Kamber, B.S. Geological and trace element evidence for a marine sedimentary environment of deposition and biogenicity of 3.45 Ga stromatolitic carbonates in the Pilbara Craton, and support for a reducing Archaean ocean. *Geobiology* **2003**, *1*, 91–108. [CrossRef]
103. Zhao, Y.Y.; Zheng, Y.F.; Chen, F.K. Trace element and strontium isotope constraints on sedimentary environment of Ediacaran carbonates in southern Anhui, South China. *Chem. Geol.* **2009**, *265*, 345–362. [CrossRef]
104. Bayon, G.; German, C.R.; Burton, K.W.; Nesbitt, R.W.; Rogers, N. Sedimentary Fe-Mn oxyhydroxides as paleoceanographic archives and the role of aeolian flux in regulating oceanic dissolved REE. *Earth Planet. Sci. Lett.* **2004**, *224*, 477–492. [CrossRef]
105. Zhao, Y.Y.; Wei, W.; Li, S.Z.; Yang, T.; Zhang, R.X.; Somerville, I.; Santosh, M.; Wei, H.T.; Wu, J.Q.; Yang, J.; et al. Rare earth element geochemistry of carbonates as a proxy for deep-time environmental reconstruction. *Paleogeogr. Paleoclimatol. Paleoecol.* **2021**, *574*, 21. [CrossRef]
106. Dehler, C.M.; Elrick, M.; Bloch, J.D.; Crossey, L.J.; Karlstrom, K.E.; Marais, D.J.D. High-resolution $\delta^{13}C$ stratigraphy of the Chuar Group (ca. 770–742 Ma), Grand Canyon: Implications for mid-Neoproterozoic climate change. *GSA Bull.* **2005**, *117*, 32–45. [CrossRef]
107. Kaufman, A.J.; Knoll, A.H. Neoproterozoic variations in the C-isotopic composition of seawater: Stratigraphic and biogeochemical implications. *Precambrian Res.* **1995**, *73*, 27–49. [CrossRef]
108. Le Guerroué, E.; Allen, P.A.; Cozzi, A. Chemostratigraphic and sedimentological framework of the largest negative carbon isotopic excursion in Earth history: The Neoproterozoic Shuram Formation (Nafun Group, Oman). *Precambrian Res.* **2006**, *146*, 68–92. [CrossRef]
109. Debruyne, D.; Hulsbosch, N.; Muchez, P. Unraveling rare earth element signatures in hydrothermal carbonate minerals using a source-sink system. *Ore Geol. Rev.* **2016**, *72*, 232–252. [CrossRef]
110. Fu, X.G.; Wang, J.; Tan, F.W.; Chen, M.; Chen, W.B. The Late Triassic rift-related volcanic rocks from eastern Qiangtang, northern Tibet (China): Age and tectonic implications. *Gondwana Res.* **2010**, *17*, 135–144. [CrossRef]
111. Fu, X.G.; Wang, M.; Zeng, S.Q.; Feng, X.L.; Wang, D.; Song, C.Y. Continental weathering and palaeoclimatic changes through the onset of the Early Toarcian oceanic anoxic event in the Qiangtang Basin, eastern Tethys. *Paleogeogr. Paleoclimatol. Paleoecol.* **2017**, *487*, 241–250. [CrossRef]
112. Nie, Y.; Fu, X.G.; Xu, W.L.; Wen, H.G.; Wang, Z.W.; Song, C.Y. Redox conditions and climate control on organic matter accumulation and depletion during the Toarcian in the Qiangtang Basin, eastern Tethys. *Int. J. Earth Sci.* **2020**, *109*, 1977–1990. [CrossRef]
113. Wang, J.A.; Fu, X.G.; Chen, W.X.; Wang, Z.J.; Tan, F.W.; Chen, M.; Zhuo, J.W. Chronology and geochemistry of the volcanic rocks in Woruo Mountain region, northern Qiangtang depression: Implications to the Late Triassic volcanic-sedimentary events. *Sci. China Ser. D-Earth Sci.* **2008**, *51*, 194–205. [CrossRef]
114. Fu, X.G.; Wang, J.; Wang, Z.J.; Chen, W.X. U-Pb Zircon Age and Geochemical Characteristics of Volcanic Rocks from the Juhua Mountain Area in the northern Qiangtang Basin, northern Xizang(Tibet). *Geol. Rev.* **2008**, *54*, 232–242, (In Chinese with English Abstract).
115. Wang, Z.J.; Wang, J.; Tan, F.W.; Fu, X.G.; Chen, W.X.; Chen, M. Geochemical characteristics of volcanic rocks of the Upper Triassic Nadi Kangri Formation in the north Qiangtang basin, Qinghai-Tibet Plateau. *Geol. Bull. China* **2008**, *27*, 83–91, (In Chinese with English Abstract).
116. Barbieri, M.; Boschetti, T.; Petitta, M.; Tallini, M. Stable isotope (^{2}H, ^{18}O and $^{87}Sr/^{86}Sr$) and hydrochemistry monitoring for groundwater hydrodynamics analysis in a karst aquifer (Gran Sasso, Central Italy). *Appl. Geochem.* **2005**, *20*, 2063–2081. [CrossRef]
117. Hao, Y.L.; Pang, Z.H.; Kong, Y.L.; Tian, J.; Wang, Y.C.; Liao, D.W.; Fan, Y.F. Chemical and isotopic constraints on the origin of saline waters from a hot spring in the eastern coastal area of China. *Hydrogeol. J.* **2020**, *28*, 2457–2475. [CrossRef]
118. Vuataz, F.-D.; Goff, F.; Fouillac, C.; Calvez, J.-Y. A strontium isotope study of the VC-1 core hole and associated hydrothermal fluids and rocks from Valles Caldera, Jemez Mountains, New Mexico. *J. Geophys. Res. Solid Earth* **1988**, *93*, 6059–6067. [CrossRef]
119. Bau, M.; Dulski, P. Distribution of yttrium and rare-earth elements in the Penge and Kuruman iron-formations, Transvaal Supergroup, South Africa. *Precambrian Res.* **1996**, *79*, 37–55. [CrossRef]
120. Bau, M. Rare-earth element mobility during hydrothermal and metamorphic fluid-rock interaction and the significance of the oxidation state of europium. *Chem. Geol.* **1991**, *93*, 219–230. [CrossRef]
121. Wang, Y.C.; Li, L.; Wen, H.G.; Hao, Y.L. Geochemical evidence for the nonexistence of supercritical geothermal fluids at the Yangbajing geothermal field, southern Tibet. *J. Hydrol.* **2022**, *604*, 22. [CrossRef]
122. Möller, P.; Dulski, P.; De Lucia, M. REY Patterns and Their Natural Anomalies in Waters and Brines: The Correlation of Gd and Y Anomalies. *Hydrology* **2021**, *8*, 116. [CrossRef]
123. Priestley, S.C.; Karlstrom, K.E.; Love, A.J.; Crossey, L.J.; Polyak, V.J.; Asmerom, Y.; Meredith, K.T.; Crow, R.; Keppel, M.N.; Habermehl, M.A. Uranium series dating of Great Artesian Basin travertine deposits: Implications for palaeohydrogeology and palaeoclimate. *Paleogeogr. Paleoclimatol. Paleoecol.* **2018**, *490*, 163–177. [CrossRef]
124. Urey, H.C. The thermodynamic properties of isotopic substances. *J. Chem. Soc.* **1947**, 562–581. [CrossRef] [PubMed]
125. Kano, A.; Kawai, T.; Matsuoka, J.; Ihara, T. High-resolution records of rainfall events from clay bands in tufa. *Geology* **2004**, *32*, 793–796. [CrossRef]

126. Chen, F.H.; Zhang, J.F.; Liu, J.B.; Cao, X.Y.; Hou, J.Z.; Zhu, L.P.; Xu, X.K.; Liu, X.J.; Wang, M.D.; Wu, D.; et al. Climate change, vegetation history, and landscape responses on the Tibetan Plateau during the Holocene: A comprehensive review. *Quat. Sci. Rev.* **2020**, *243*, 21. [CrossRef]
127. Dykoski, C.A.; Edwards, R.L.; Cheng, H.; Yuan, D.; Cai, Y.; Zhang, M.; Lin, Y.; Qing, J.; An, Z.; Revenaugh, J. A high-resolution, absolute-dated Holocene and deglacial Asian monsoon record from Dongge Cave, China. *Earth Planet. Sci. Lett.* **2005**, *233*, 71–86. [CrossRef]
128. Wang, Y.; Cheng, H.; Edwards, R.L.; He, Y.; Kong, X.; An, Z.; Wu, J.; Kelly, M.J.; Dykoski, C.A.; Li, X. The Holocene Asian Monsoon: Links to Solar Changes and North Atlantic Climate. *Science* **2005**, *308*, 854–857. [CrossRef]